Elsevier Editorial System(tm) for Materials Letters or its open access mirror
Manuscript Draft

Manuscript Number: MLBLUE-D-20-02907R1

Title: Heat treatment effect on an AA6063 alloy

Article Type: Short Communication

Keywords: Microstructure; strength contributions; aging treatment; defects.

Corresponding Author: Dr. Jairo Alberto Muñoz Bolaños, Ph.D

Corresponding Author's Institution: National University of Science and Technology MISiS

First Author: Jairo Alberto Muñoz Bolaños, Ph.D

Order of Authors: Jairo Alberto Muñoz Bolaños, Ph.D; Alexander Komissarov; Martina Avalos; Raúl E Bolmaro

Abstract: The aging treatment effect on an AA6063 aluminum alloy was studied by characterizing the microstructure and mechanical properties. The aging impact increased the alloy strength from 100 MPa in the solubilization state to 200 MPa in the aged state. The aging treatment effect, in addition to the formation of precipitates, gave rise to a high number of geometrically necessary dislocations at (GND), and different concentrations of Si and Mg inside some grains. The early fracture of the aged material concerning the solubilization condition was demonstrated by the multiple formations of strain peaks and a high dislocation annihilation rate. The most significant strength contributions to the aged alloy came from precipitates, followed by the solid solution, dislocations, and grain size.

Research Data Related to this Submission

There are no linked research data sets for this submission. The following reason is given:
Data will be made available on request

Dr. Jairo Alberto Muñoz Bolaños
Instituto Física de Rosario, Universidad Nacional de Rosario, Bv. 27 de Febrero, S2000EKF Rosario, Santa Fe, Argentina.
National University of Science and Technology "MISIS", Moscow 119049, Russia
E-mail: jairomunoz8614@gmail.com
Tel.: +79161624057

Prof. Dr. Boris Borisovich Straumal
Editor of the Journal Materials Letters

July 10, 2020

Subject: Revision manuscript: MLBLUE-D-20-02907

Dear Professor,

Please find in attached files of our manuscript entitled **" Heat treatment effect on an AA6063 alloy "** to be submitted electronically for publication in the Journal Materials Letters. The manuscript has not been published before and is not currently submitted for publication to any other journal and will not be submitted elsewhere before a decision is made by this journal. This research work has been revised and approved by all the co-authors and institutions.

We appreciate the detailed comments by the reviewer and the editor. They raised new topics that enriched the content of the paper. Our responses are marked in Italics below and the changes in the manuscript are marked using yellow highlighting.

Reviewers and editor comments:

1) **It is a good paper devoted to the very important material, namely the AA6063 Al-based alloy. Due to the alloying elements, mechanical strength of Al-alloys can be improved by additional hardening mechanisms other than dislocations, such as the solid solution of the alloying elements with the aluminum matrix and the formation of precipitates between the alloying elements. The paper could be published after moderate revisions. In particular, the authors studied the difference in structura and properties between one-phase state of the AA6063 alloy after its homogenization at 530oC and the multiphase state of the same alloy after its additional ageing at 190oC. The authors observe that XRD patterns of the alloy after homogenization contain only narrow peaks of the fcc phase. After additional ageing the small peaks of the intermetallic phase become visible, the fcc peaks broaden and the strong underground appears. The fcc peaks also shift to the lower diffraction**
angles. This fact manifests the "purification" of Al-based matrix from the alloying elements. Behing these phenomena, the formation of thin layers of various grain boundary phases

enriched on Mg and other alloying elements can be hidden (see for example Adv Eng Mater17 (2015) 1821). Such redistribution of alloying components between matrix solid solution and the segregation layers of grain boundary phases can, in turn, strongly modify the kinetic properties of grain boundaries and overall mechanical properties of the alloy (see for example Mater. Lett. 84 (2012) 63). The grain boundary segregation and grain boundary phases can definitely influence the phenomena observed by the authors. I would strongly propose to discuss these points in the paper.

Answer: *Thank you for the comments. Some paragraphs describing the new points suggested by the editor and reviewers have been added into the manuscript at different points in the results and discussion section.*

1)

Fig. 1c shows the characteristic peaks of aluminum as well as Mg_2Si, AlMnSi, and AlMn intermetallic precipitates, with higher intensity for the aged material, in agreement with other

investigations in 6XXX series alloys [9,10]. The precipitation formation and the peaks broadening in the T6 material also indicate the Al matrix purification [11]. Through Figs. 1d-1f, the formation of different precipitates inside grains and along grain boundaries is corroborated. The EDS spectra for a precipitate within a grain (Fig. 1e) with an elongated shape shows a Mg and Si-rich composition, while in the grain boundary area, Si and Mn predominate (Fig. 1f).

2)

The highest GND of the T6 material are associated with the more significant presence of precipitates and higher concentrations of alloying elements inside some grains leading not only to higher strength but also to better capacity for grain refinement (i.e., GND grouping). Fig. 2e illustrates a detailed image quality and GND map. Fig. 2f shows the EDS mapping for Mg and Si in which the highest concentrations of Si corresponds with the zones of low image quality and high GNDs densities. At the same time, Mg distributed over the entire Al matrix does not present an apparent relationship with the GNDs values. Fig. 2e also highlights some Mg and Si-rich precipitates not correlating with image quality values. Therefore, Si affects more the

microstructure than Mg. The GNDs heterogeneity and low misorientations can be due to the segregation by thin layers of grain boundaries enriched in Mg and Si, which modify the grain boundaries' kinetics and the mechanical properties of the alloy [12].

3)

Kocks-Mecking-Estrin (KME) model, information on the evolution of the dislocation can be assessed by following the equation (2) [15]:

$$\frac{\partial \rho}{\partial \varepsilon} = M(K_1\sqrt{\rho} - K_2\rho) \qquad (3)$$

with K_1 y K_2 constants related to the storage and annihilation of dislocations, respectively.

The KME model shows a good fit with the experimental values of Fig. 3a, besides, Fig. 3b allows observing an increasing number of dislocations with similar values at the beginning of the deformation (i.e., K_1 and K_2 similar). However, at higher strains, a decrease in the growth rate of dislocations is observed for the T6 material matching the higher value of K_2, as indicated in Table 1. The lower hardening in the aged material can be associated with a higher degree of purification, giving rise to grain boundaries enriched in Mg and Si that restrict the free movement of dislocations [11]. The strain maps in Figs. 3c-3d proves the better ductility of the ST material. These figures display a strain concentration in a small band, which changes place with larger applied strains, while the T6 material indicates in Figs. 3e-3f a different behavior, with the formation of multiple strain peaks resulting in an earlier fracture. These strain

Yours sincerely

Dr. Jairo Alberto Muñoz Bolaños

Corresponding author
On behalf of all authors.

Graphical Abstract

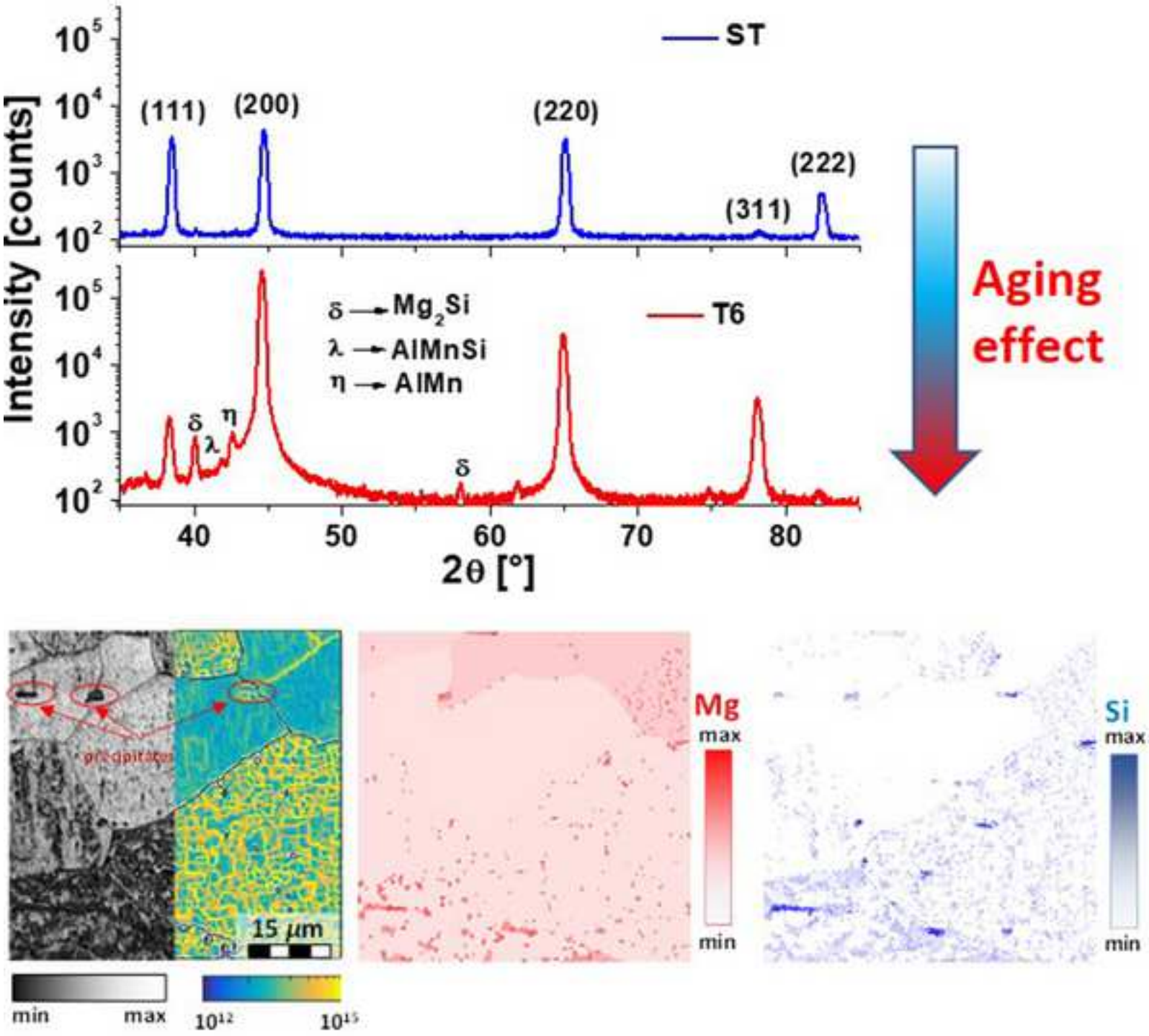

Highlights

• Strength improvement was penalized by ductility reduction after aging treatment.

• Heterogeneous distributions of geometrically necessary dislocations after the aging heat treatment.

• High dislocation annihilation rate after aging treatment during the tensile test.

• High Silicon concentrations inside some grains are the main responsible for high misorientations after aging treatment.

• Multiple strain peaks during the tensile test for the aged material gave rise to an early fracture.

Heat treatment effect on an AA6063 alloy

Jairo Alberto Muñoz[1, 2, a], Alexander Komissarov[2], Martina Avalos[1], Raúl E. Bolmaro[1].

[1]Instituto de Física Rosario, Consejo Nacional de Investigaciones Científicas y Técnicas-CONICET, Universidad Nacional de Rosario, Ocampo y Esmeralda, 2000 Rosario, Argentina
[2]National University of Science and Technology "MISIS", Moscow 119049, Russia.

[a]munoz@ifir-conicet.gov.ar

Abstract

The aging treatment effect on an AA6063 aluminum alloy was studied by characterizing the microstructure and mechanical properties. The aging impact increased the alloy strength from 100 MPa in the solubilization state to 200 MPa in the aged state. The aging treatment effect, in addition to the formation of precipitates, gave rise to a high number of geometrically necessary dislocations at (GND), and different concentrations of Si and Mg inside some grains. The early fracture of the aged material concerning the solubilization condition was demonstrated by the multiple formations of strain peaks and a high dislocation annihilation rate. The most significant strength contributions to the aged alloy came from precipitates, followed by the solid solution, dislocations, and grain size.

Keywords: *Microstructure, strength contributions, aging treatment, defects.*

1 Introduction

Unlike pure aluminum, aluminum alloys show a wide variety of structural properties (e.g., corrosion resistance, mechanical strength, good weldability, formability, among others) allowing for applications in a wide variety of industries such as automotive, aeronautics, sports, and civil [1]. Due to the alloying elements, mechanical strength is improved by additional hardening mechanisms other than dislocations, such as the solid solution of the alloying elements with the aluminum matrix and the formation of precipitates between the alloying elements. [2,3]. E.g., silicon helps to generate high dislocation densities, while it also influences the material ductility reduction. It has also been shown how the Mg/Si ratio controls the hardness of the material so that a Mg excess (i.e., Mg/Si >1.7) helps to keep its value constant after aging [4].

Alloys corresponding to Al-Mg-Si system (or 6XXX series) can be subject to heat treatments such as quenching and artificial aging for improving their mechanical strengths [5]. However, the strength increase is penalized with material ductility reduction after aging treatment, making these types of alloys prone to failure by deformation [6]. For this reason, knowing the microstructural characteristics (e.g., grain size, dislocation density, texture, misorientation, and precipitates) as well as their configuration and distribution is of vital importance to define the final mechanical response of metallic materials under tensile, fatigue, and fracture toughness requirements.

The main goal of this manuscript is to reveal the heat treatment effect on the microstructure and deformation behavior of AA6063 aluminum alloy under solubilization and aging states using scanning electron microscopy and strain maps obtained with digital image correlation during uniaxial tensile tests.

2 Experimental procedure

The material is an AA6063 alloy with the following composition (wt%): (0.45–0.9%Mg; 0.2–0.6%Si; 0.1%Cr; 0.1%Zn; 0.35%Fe; 0.1%Mn; 0.1%Ti; 0.1%Cu;). It was solubilized at 530 °C for 4 h and water quenched (ST). Additionally, after solubilization, it was aged at 190 °C for 10 h and air-cooled (T6). Microstructural characterization was performed by electron back-scattering diffraction (EBSD) and electron dispersion spectroscopy (EDS), an integrated TSL-OIM EDAX EBSD system mounted on a FEG SEM Quanta 200 electron microscope, Digi-View camera and TSL OIM 7.3 post-processing tool. Pole figures were obtained with a Cu-Kα (1.5405 Å) radiation, X-ray lenses, parallel plate collimator, and Xe detector diffractometer. Subsequently, they were corrected, analyzed, and recalculated by using WXpopLA [7]. The diffractograms were measured in the 2θ range of 34° -87° with a step of 0.02°. Material strength was evaluated with uniaxial tensile tests at constant strain rate 1.1×10^{-3} s^{-1} on samples of 12mm × 3mm × 3mm.

3 Results and analysis

Fig. 1 represents the microstructure characterization of the material in ST and T6 conditions. Fig. 1a-Fig. 1b show the microstructure before and after aging does not register substantial changes regarding its grain size and texture. Table 1 shows that the T6 material has a slightly smaller grain size than the ST material, i.e. 74.4 μm and 80.5 μm, respectively. The texture of both materials indicates a clear orientation with direction [001] parallel to the rolling

direction (RD) with a clear prevalence of Cube and some Goss components, which are mainly associated with recrystallization phenomena [8].

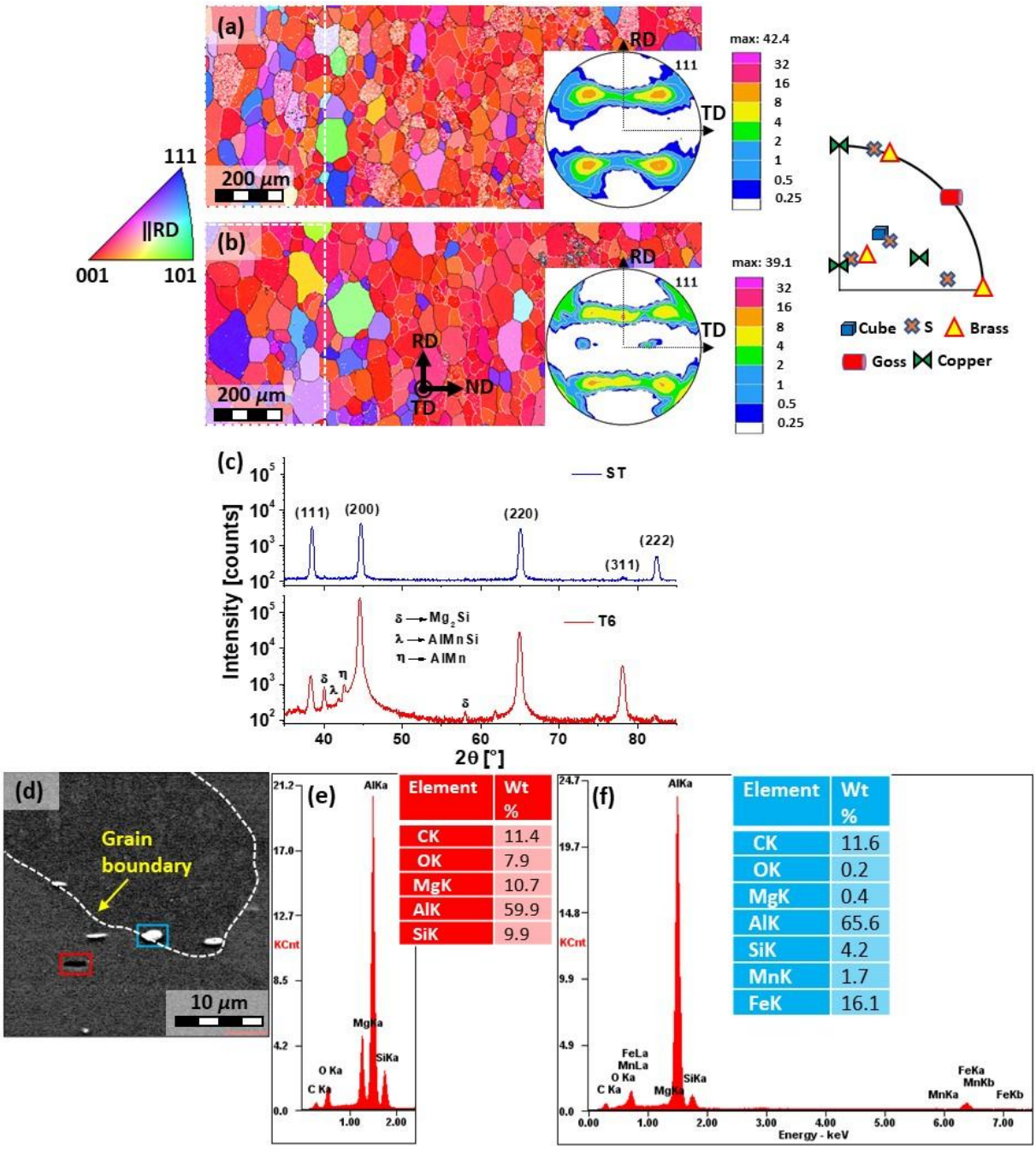

Fig. 1. Microstructure characterization, inverse pole figure maps and PF for (a) T6 material, (b) ST material, (c) x-ray diffractograms, (d) EDS zone, and EDS spectrums for (e) red square, and (f) blue square. 10^6 pixel scans were taken in a hexagonal grid.

Fig. 1c shows the characteristic peaks of aluminum as well as Mg_2Si, AlMnSi, and AlMn intermetallic precipitates, with higher intensity for the aged material, in agreement with other

investigations in 6XXX series alloys [9,10]. The precipitation formation and the peaks broadening in the T6 material also indicate the Al matrix purification [11]. Through Fig. 1d-Fig. 1f, the formation of different precipitates inside grains and along grain boundaries is corroborated. The EDS spectra for a precipitate within a grain (Fig. 1e) with an elongated shape shows a Mg and Si-rich composition, while in the grain boundary area, Si and Mn predominate (Fig. 1f).

Table 1. Material properties

Material	Grain size [μm]	HAGB	Crystal Size [m]	Dislocations x-ray [m^{-2}]	σ_0 [MPa]	σ_{SS} [MPa]	σ_{pp} [MPa]	σ_{GB} [MPa]	σ_ρ [MPa]	K_1 [m^{-1}]	K_2
ST	80.5	0.44	6.6×10^{-7}	3.1×10^{13}	10	56±17	.....	12.7	30.7	1.5×10^{9}	61.2
T6	74.4	0.25	5.9×10^{-7}	4.7×10^{13}	10	56±17	83.8	13.2	37.3	1.9×10^{9}	101.6

Fig. 2a and Fig. 2b indicate the GNDs maps for the T6 and ST materials corresponding to the areas delimited by the white dashed line square in Fig. 1a, respectively. At first glance, it is noted that in the T6 material, there are some grains with high densities of GNDs forming boundaries, while in the other grains, dislocations are evenly distributed as in the ST material. Looking in detail inside some grains, Fig. 2c plots the misorientation profiles along the red lines 1 and 2 on the GND maps. These profiles demonstrate that the most of GNDs are associated with lower misorientations because of the higher subgrain fractions in the T6 than for the ST material. This behavior of condition T6 also generates a change in the global distribution of GNDs, as indicated in Fig. 2d. This figure demonstrates how the material T6 registers GND densities higher than ST with dislocation fractions beyond 3×10^{13} m^{-2}, giving rise to a higher average value in the T6 condition than in the ST material.

The highest GND of the T6 material are associated with the more significant presence of precipitates and higher concentrations of alloying elements inside some grains leading not only to higher strength but also to better capacity for grain refinement (i.e., GND grouping). Fig. 2e illustrates a detailed image quality and GND map. Fig. 2f shows the EDS mapping for Mg and Si in which the highest concentrations of Si corresponds with the zones of low image quality and high GNDs densities. At the same time, Mg distributed over the entire Al matrix does not present an apparent relationship with the GNDs values. Fig. 2e also highlights some Mg and Si-rich precipitates not correlating with image quality values. Therefore, Si affects

more the microstructure than Mg. The GNDs heterogeneity and low misorientations can be due to the segregation by thin layers of grain boundaries enriched in Mg and Si, which modify the grain boundaries' kinetics and the mechanical properties of the alloy [12].

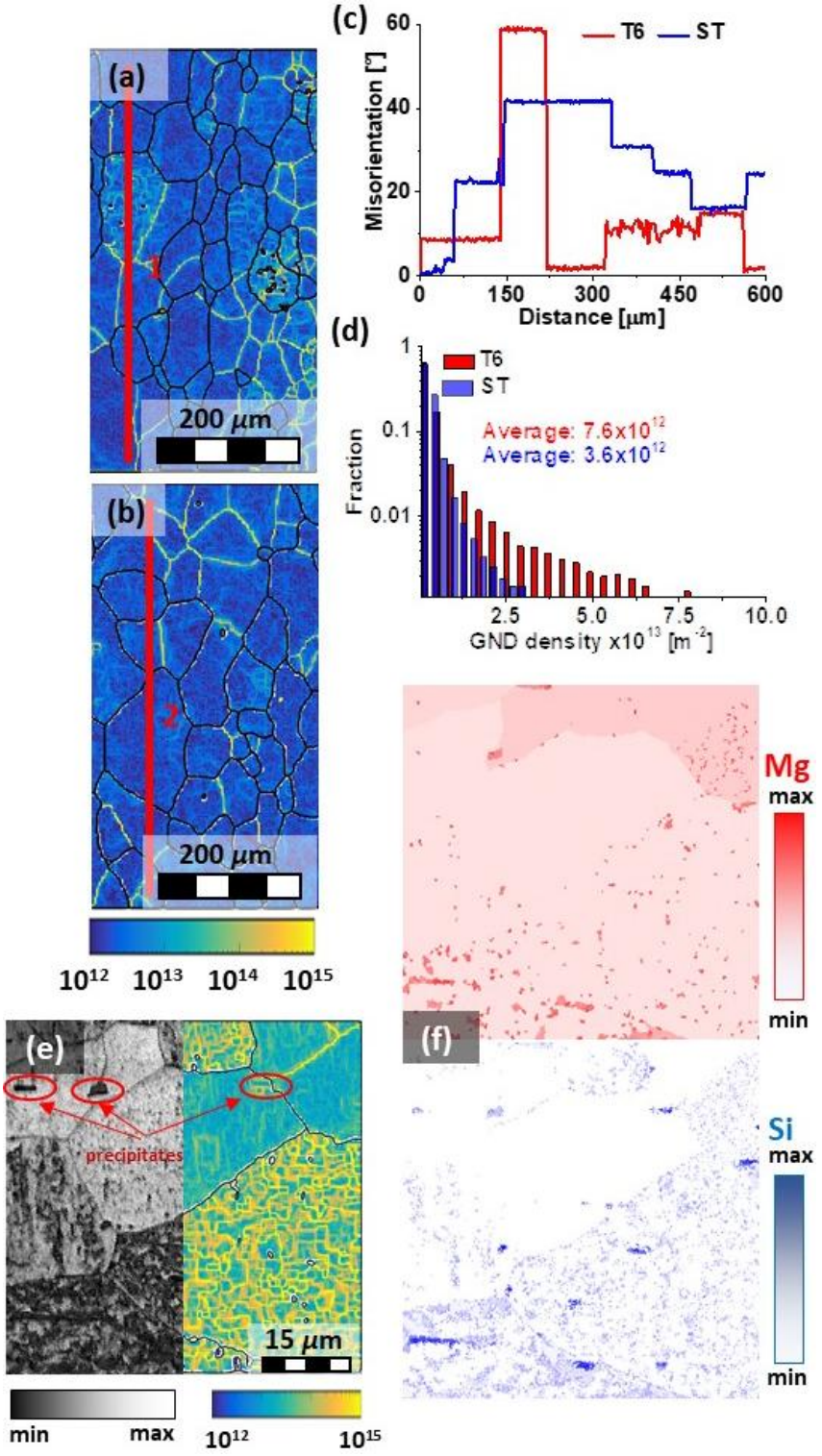

Fig. 2. GND for (a) T6, (b) ST, (c) misorientation profile for the red lines 1 and 2 in the GND maps, (d) GND distributions, (e) detail EBSD map, and (f) corresponding Mg and Si EDS mapping.

Al alloys strengthening mechanisms consider the solid solution (σ_{ss}), precipitates (σ_{pp}), grain size (σ_{GB}) and dislocations (σ_{ρ}) contributions as indicated by equation (1) [2]:

$$\sigma_y = \sigma_0 + \sigma_{ss} + \sigma_{pp} + \sigma_{GB} + \sigma_{\rho} \quad (1)$$

where $\sigma_0 \cong 10$ MPa is the friction stress [13]. $\sigma_{ss} = \sum_j k_j c_j^{2/3}$ (j = Mg, Si), c the wt% of each element, k a constant of 29 MPa/(wt%)$^{2/3}$ for Mg and 66.3 MPa/(wt%)$^{2/3}$ for Si [4]. $\sigma_{GB} = k_{HP}\left(\frac{1}{d}\right)^{1/2}$ with k_{HP} = 0.114 MPa m$^{1/2}$ [14], and d the grain size. $\sigma_{\rho} = M\alpha bG\sqrt{\rho}$ where M=3.06 is the Taylor factor, α=0.24, b=2.86· 10^{-10} m the Burgers vector, G=26 GPa the shear module, and ρ the dislocation density obtained by x-ray diffraction following the equation [10]:

$$\rho = \frac{2\sqrt{3}\langle\varepsilon^2\rangle^{1/2}}{Db} \quad (2)$$

With ε and D as the microstrain and the crystal size, respectively.

Thus, the precipitation contribution is estimated from the difference between the yield stress and the strength contributions using equation (**1**) and is summarized in Table 1. Using the Kocks-Mecking-Estrin (KME) model, information on the evolution of the dislocation can be assessed by following the equation (3) [15]:

$$\frac{\partial\rho}{\partial\varepsilon} = M(K_1\sqrt{\rho} - K_2\rho) \quad (3)$$

with K_1 y K_2 constants related to the storage and annihilation of dislocations, respectively.

The KME model shows a good fit with the experimental values of Fig. 3a, besides, Fig. 3b allows observing an increasing number of dislocations with similar values at the beginning of the deformation (i.e., K_1 and K_2 similar). However, at higher strains, a decrease in the growth rate of dislocations is observed for the T6 material matching the higher value of K_2, as indicated in Table 1. The lower hardening in the aged material can be associated with a higher degree of purification, giving rise to grain boundaries enriched in Mg and Si that restrict the free movement of dislocations [11]. The strain maps in Fig. 3c-Fig. 3d proves the better ductility of the ST material. These figures display a strain concentration in a small band, which changes place with larger applied strains, while the T6 material indicates in Fig. 3e-Fig.

3f a different behavior, with the formation of multiple strain peaks resulting in an earlier fracture. These strain concentrations can be related to the heterogeneous distribution of Si inside some grains of the T6 microstructure creating potential strain concentration points. In this way, Si content seems to play a more critical role in defining the mechanical response of the AA6063 alloy than Mg.

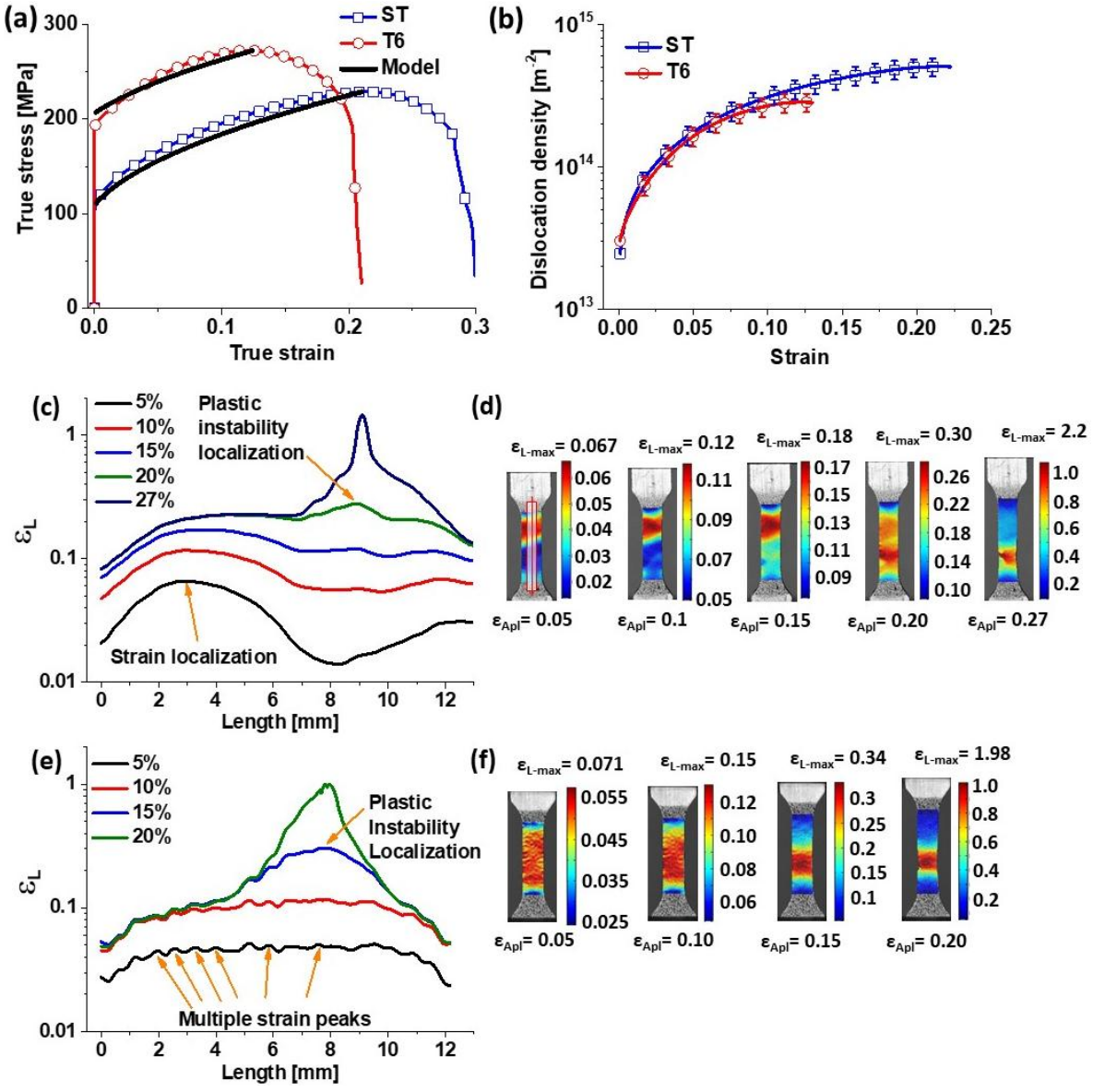

Fig. 3. (a) Tensile curves, (b) dislocation density, (c) ST ε_L strain evolution for different ε_{Apl}, (d) ST strain maps, (e), T6 ε_L strain evolution for different ε_{Apl} and (f) T6 strain maps.

4 Conclusions

Aging treatment resulted in a strength increase due to the contribution of precipitates, solid solution highlighting higher amounts of Si in some grains, and high dislocations forming boundaries than create low misorientations across the microstructure.

The lower ductility of the T6 material is related to two factors: 1) higher rate of dislocation annihilation, as demonstrated by the KME model, 2) more prominent amounts of Si inside some grains, making them potential sites for strain concentration, which give rise to the formation of multiple strain peaks during the tensile test. In contrast, the ST material concentrates the strain at specific zones that change its place with deformation.

Acknowledgments

JAMB acknowledges the financial support of the Ministry of Science and Higher Education of the Russian Federation in the framework of Increase Competitiveness Program of NUST «MISiS» (№ К4-2019-045), implemented by a governmental decree dated 16th of March 2013, N 211.

References

[1] L.P. Troeger, E.A. Starke, Mater. Sci. Eng. A 277 (2000) 102–113.
[2] Y. Chen, N. Gao, G. Sha, S.P. Ringer, M.J. Starink, Acta Mater. 109 (2016) 202–212.
[3] S.K. Panigrahi, R. Jayaganthan, Mater. Sci. Eng. A 528 (2011) 3147–3160.
[4] S. Jiang, R. Wang, J. Mater. Sci. Technol. 35 (2019) 1354–1363.
[5] S.K. Panigrahi, R. Jayaganthan, J. Alloys Compd. 470 (2009) 285–288.
[6] Y. Wang, H. Liao, Y. Wu, J. Yang, Mater. Des. 53 (2014) 634–638.
[7] J.S. Kallend, U.F. Kocks, A.D. Rollett, H.-R. Wenk, Mater. Sci. Eng. A 132 (1991) 1–11.
[8] J.A. Muñoz, M. Avalos, R.E. Bolmaro, J. Alloys Compd. 768 (2018) 349–357.
[9] T. Khelfa, J.A. Muñoz-Bolaños, F. Li, J.M. Cabrera-Marrero, M. Khitouni, Met. Mater. Int. (2019).
[10] T. Khelfa, M.A. Rekik, M. Khitouni, J.M. Cabrera-Marrero, Int. J. Adv. Manuf. Technol. 92 (2017) 1731–1740.
[11] A.A. Mazilkin, B.B. Straumal, M. V Borodachenkova, R.Z. Valiev, O.A. Kogtenkova, B. Baretzky, Mater. Lett. 84 (2012) 63–65.
[12] X. Sauvage, M.Y. Murashkin, B.B. Straumal, E. V Bobruk, R.Z. Valiev, Adv. Eng. Mater. 17 (2015) 1821–1827.
[13] P. Snopiński, M.Ó. Kr, Metals (Basel). 8 (2018).
[14] T. Khelfa, M.A. Rekik, J.A. Muñoz-Bolaños, J.M. Cabrera-Marrero, M. Khitouni, Int. J. Adv. Manuf. Technol. 95 (2017) 1165–1166.
[15] Y. Estrin, J. Mater. Process. Technol. 80–81 (1998) 33–39.

Figure 1

Click here to download high resolution image

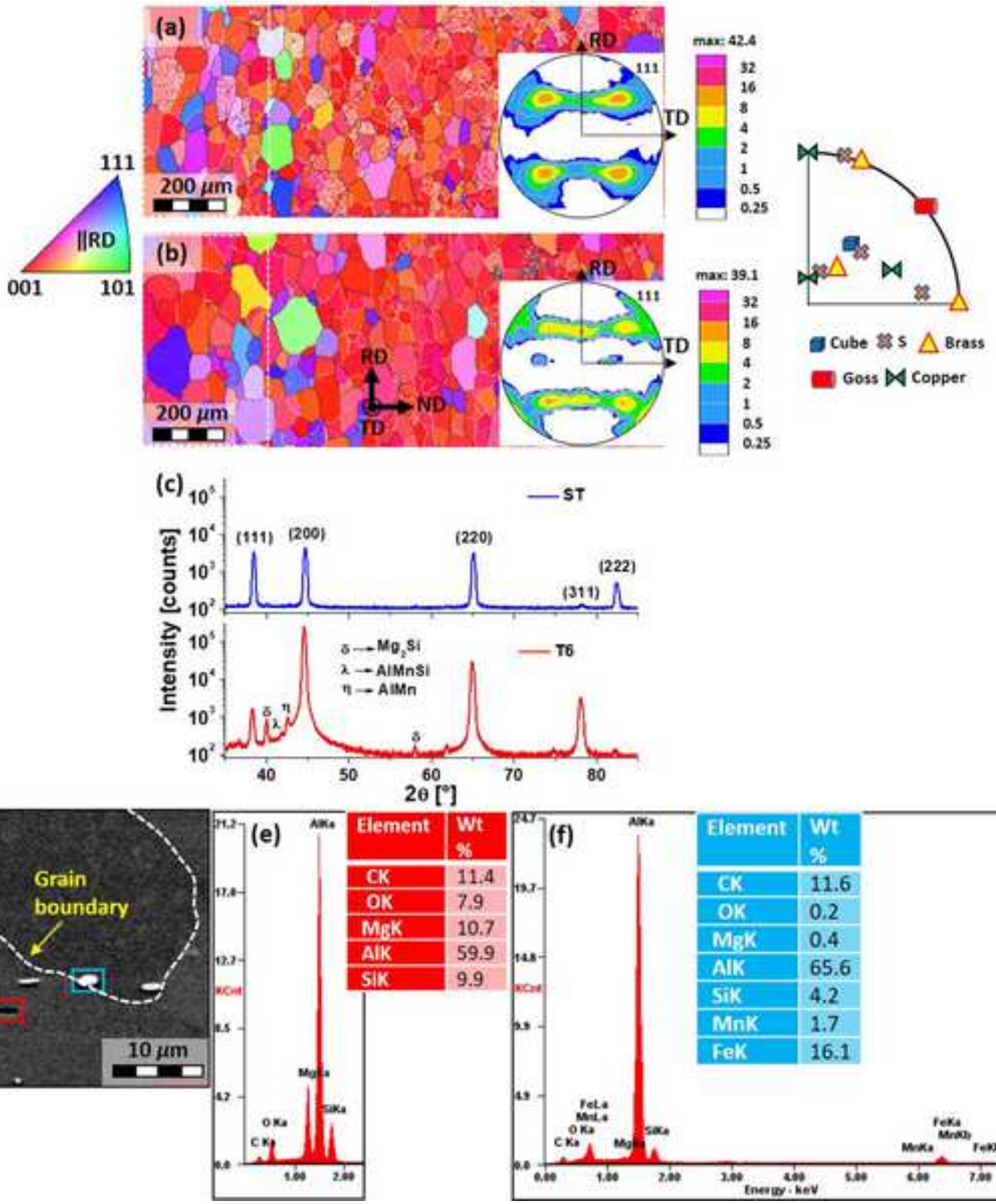

Element	Wt %
CK	11.4
OK	7.9
MgK	10.7
AlK	59.9
SiK	9.9

Element	Wt %
CK	11.6
OK	0.2
MgK	0.4
AlK	65.6
SiK	4.2
MnK	1.7
FeK	16.1

Figure 2

Click here to download high resolution image

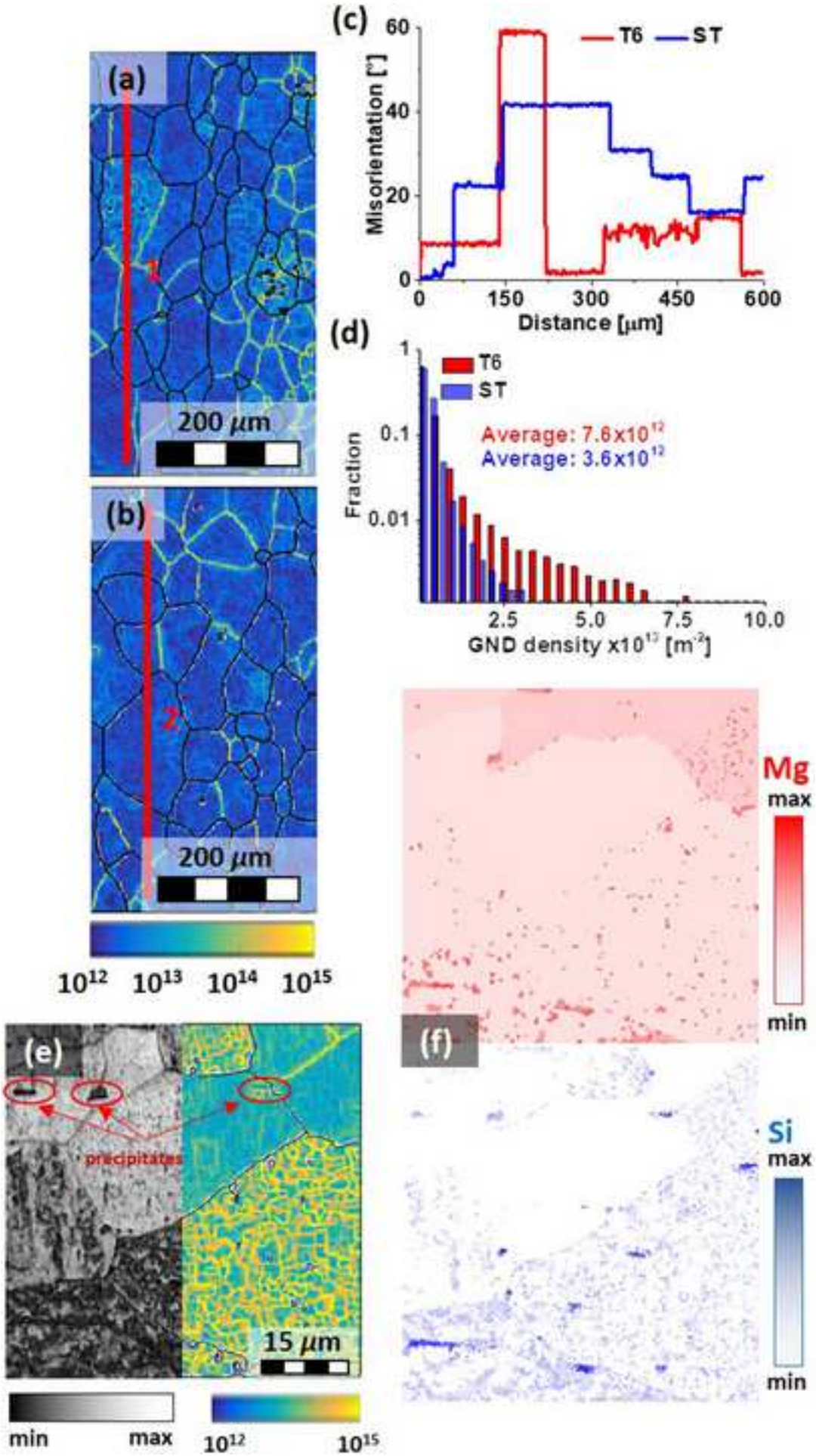

Figure 3

Click here to download high resolution image

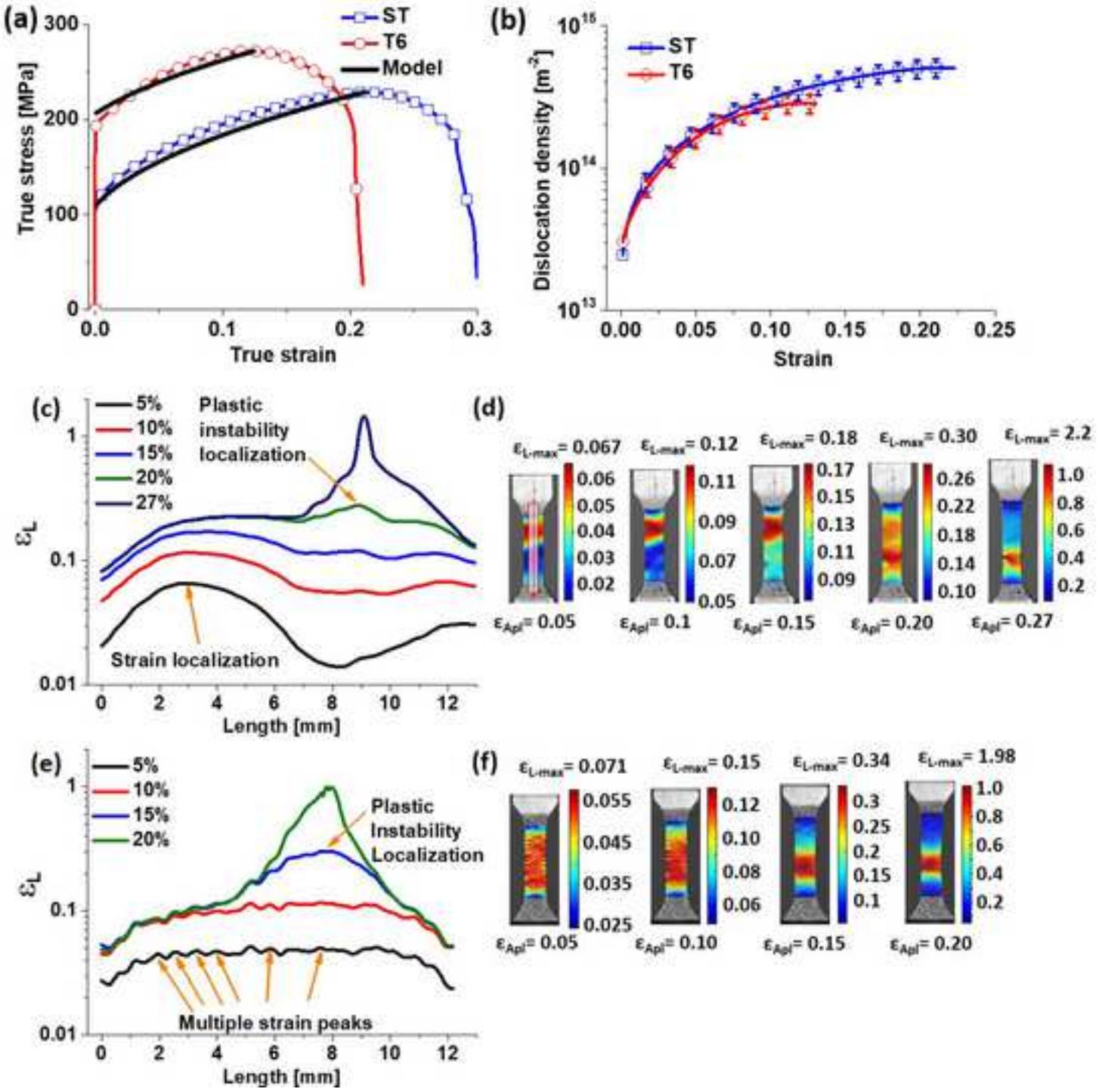

Table

Table 1. Material properties

Material	Grain size [μm]	HAGB	Crystal Size [m]	Dislocations x-ray [m^{-2}]	σ_0 [MPa]	σ_{SS} [MPa]	σ_{pp} [MPa]	σ_{GB} [MPa]	σ_ρ [MPa]	K_1 [m^{-1}]	K_2
ST	80.5	0.44	6.6×10^{-7}	3.1×10^{13}	10	56±17	.....	12.7	30.7	1.5×10^{9}	61.2
T6	74.4	0.25	5.9×10^{-7}	4.7×10^{13}	10	56±17	83.8	13.2	37.3	1.9×10^{9}	101.6

***Declaration of Interest Statement**

Declaration of interests

☒ The authors declare that they have no known competing financial interests or personal relationships that could have appeared to influence the work reported in this paper.

☐The authors declare the following financial interests/personal relationships which may be considered as potential competing interests:

***Conflict of Interest**

Click here to download Conflict of Interest: Conflict of interest.docx

Credit authorship contribution statement

Jairo Alberto Muñoz: Investigation, formal analysis, writing original draft, writing review and editing **Alexander Komissarov:** Supervision, investigation. **Martina Avalos:** Supervision, funding acquisition, formal analysis. **Raúl E. Bolmaro:** Supervision, writing review and editing, resources, project administration, funding acquisition.